Journal of Controlled Release 152 (2011) 76–83

Contents lists available at ScienceDirect

Journal of Controlled Release

journal homepage: www.elsevier.com/locate/jconrel

Doxorubicin loaded iron oxide nanoparticles overcome multidrug resistance in cancer *in vitro*

Forrest M. Kievit [a], Freddy Y. Wang [a], Chen Fang [a], Hyejung Mok [a], Kui Wang [a], John R. Silber [b], Richard G. Ellenbogen [b], Miqin Zhang [a,b,*]

[a] Department of Materials Science and Engineering, University of Washington, Seattle, WA 98195, USA
[b] Department of Neurological Surgery, University of Washington, Seattle, WA 98195, USA

ARTICLE INFO

Article history:
Received 29 October 2010
Accepted 19 January 2011
Available online 26 January 2011

Keywords:
Brain tumors
Chemotherapy
Drug efflux
Theranostics
Glioma

ABSTRACT

Multidrug resistance (MDR) is characterized by the overexpression of ATP-binding cassette (ABC) transporters that actively pump a broad class of hydrophobic chemotherapeutic drugs out of cancer cells. MDR is a major mechanism of treatment resistance in a variety of human tumors, and clinically applicable strategies to circumvent MDR remain to be characterized. Here we describe the fabrication and characterization of a drug-loaded iron oxide nanoparticle designed to circumvent MDR. Doxorubicin (DOX), an anthracycline antibiotic commonly used in cancer chemotherapy and substrate for ABC-mediated drug efflux, was covalently bound to polyethylenimine via a pH sensitive hydrazone linkage and conjugated to an iron oxide nanoparticle coated with amine terminated polyethylene glycol. Drug loading, physiochemical properties and pH lability of the DOX-hydrazone linkage were evaluated *in vitro*. Nanoparticle uptake, retention, and dose-dependent effects on viability were compared in wild-type and DOX-resistant ABC transporter over-expressing rat glioma C6 cells. We found that DOX release from nanoparticles was greatest at acidic pH, indicative of cleavage of the hydrazone linkage. DOX-conjugated nanoparticles were readily taken up by wild-type and drug-resistant cells. In contrast to free drug, DOX-conjugated nanoparticles persisted in drug-resistant cells, indicating that they were not subject to drug efflux. Greater retention of DOX-conjugated nanoparticles was accompanied by reduction of viability relative to cells treated with free drug. Our results suggest that DOX-conjugated nanoparticles could improve the efficacy of chemotherapy by circumventing MDR.

1. Introduction

Treatment of approximately 50% of human cancers includes the use of chemotherapy [1]. In many instances, the effectiveness of chemotherapy is limited by selection of drug-resistant cells expressing the multidrug resistance (MDR) phenotype. MDR generally reflects the overexpression of ATP-binding cassette (ABC) transporters which increase the efflux of a broad class of hydrophobic drugs from cancer cells [2]. While significant effort has been placed on the discovery and development of MDR inhibitors, their clinical application has been hindered by low efficacy and high toxicity [2]. This has provided a strong incentive for researchers to develop other strategies to overcome MDR.

Nanotechnology provides an alternative strategy to circumvent MDR by offering a means to encapsulate or attach drugs to nanomaterials such as lipids, polymers and solid-core nanoparticles which are resistant to drug efflux. Conjugation to nanomaterials can also maximize exposure of target cells to drug by prolonging drug persistence in the circulation and enhancing penetration of physiological barriers. Inclusion of targeting ligands has the potential of effecting tumor-specific drug delivery and retention, thus minimizing systemic toxicity [3–5].

Early nanotechnology strategies for overcoming MDR included loading drug into liposomes in order to increase drug concentration in the tumor [6]. This has led to the development of liposome encapsulated doxorubicin (DOX; trade names Doxil, Caelyx, and Myocet), and daunorubicin (DaunoXome), two anthracycline antibiotics commonly used in cancer chemotherapy. However, these lipid-encapsulated anthracyclines have limited clinical utility and are used primarily in the treatment of breast cancer and AIDS-related Kaposi sarcoma and multiple myeloma [7]. Furthermore, in an early study, liposome encapsulated DOX was subject to MDR in glioma cells [8]. An improved lipid nanocapsule formulation containing paclitaxel was developed and showed improved resistance to MDR in a rodent

Abbreviations: MDR, multidrug resistance; DOX, doxorubicin; ABC, ATP-binding cassette; SPION, superparamagnetic iron oxide nanoparticle; NP, nanoparticle; NP-DOX, nanoparticle-doxorubicin conjugate.

* Corresponding author at: Department of Materials Science and Engineering, University of Washington, 302L Roberts Hall, Box 352120, Seattle, WA 98195, USA. Tel.: +1 206 616 9356; fax: +1 206 543 3100.
E-mail address: mzhang@u.washington.edu (M. Zhang).

0168-3659/$ – see front matter © 2011 Elsevier B.V. All rights reserved.
doi:10.1016/j.jconrel.2011.01.024

glioma model [9]. These results indicate that encapsulating drugs in nanomaterials is a promising strategy for overcoming MDR. Other early nanotechnology approaches for overcoming MDR in cancer include covalent attachment of drug to polymers and solid-core nanoparticles to prevent drug efflux [10,11].

Superparamagnetic iron oxide nanoparticles (SPIONs) have emerged as a promising nanomaterial for drug delivery due to their ability for integrative therapeutic and diagnostic (i.e. theranostic) applications [5,12–14]. The superparamagnetism of the iron oxide core enhances contrast in magnetic resonance imaging (MRI) facilitating

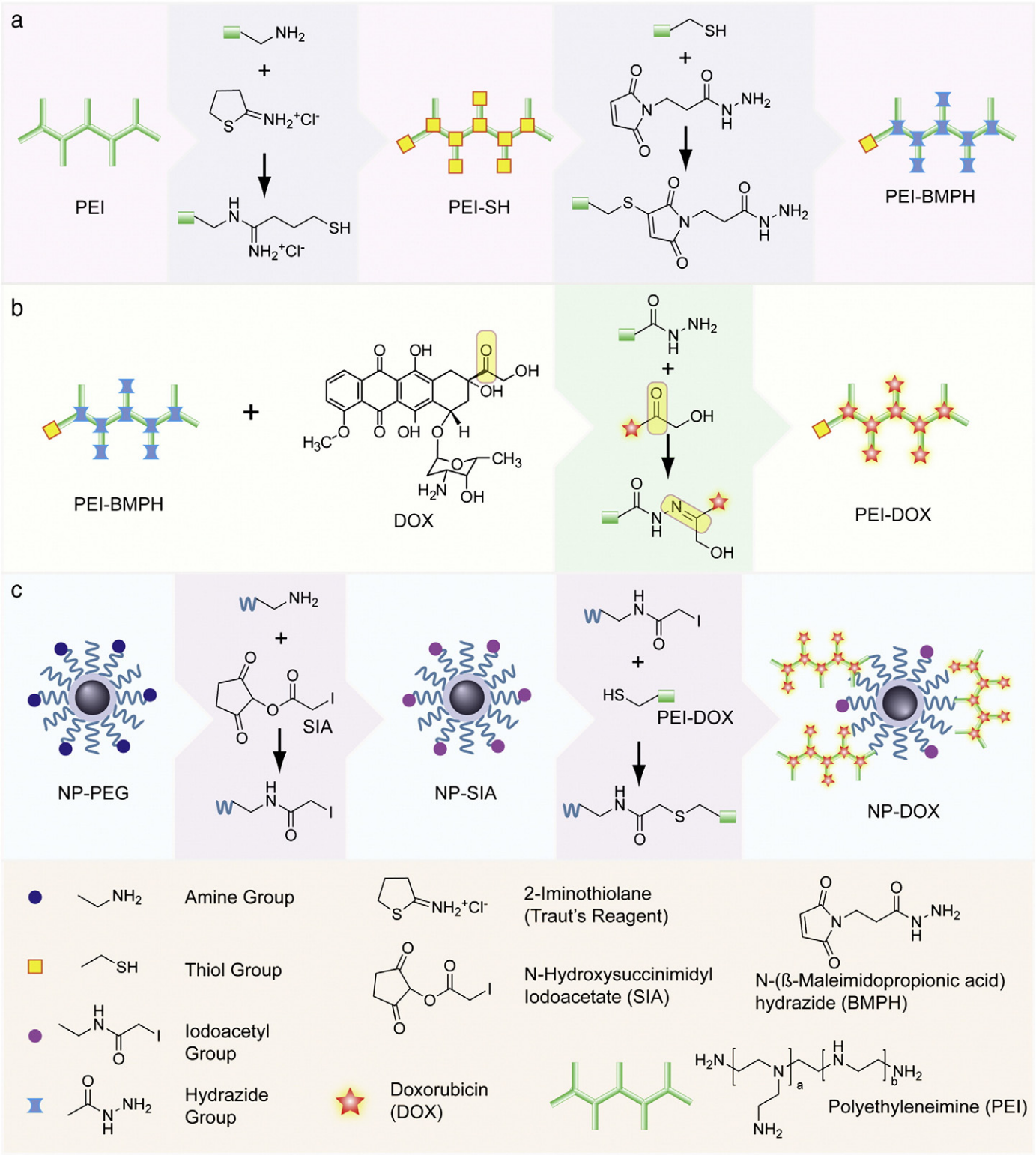

Fig. 1. Synthesis schematic. a) Polyethylenimine (PEI) was activated with a hydrazine group through subsequent modifications with Traut's reagent and BMPH to form PEI-BMPH. b) Doxorubicin (DOX) was attached to PEI-BMPH through a hydrazone bond. c) Amine terminated PEG coated iron oxide nanoparticles (NP-PEG) were activated with SIA to render a free iodoacetyl group and subsequently reacted to PEI-DOX through a thioether linkage to form NP-DOX. Each NP-DOX had 216 ± 99 PEI, and 5 ± 2 DOX per PEI.

non-invasive, real-time monitoring of drug delivery. This could allow physicians the ability to adjust dosing to achieve optimal tumor uptake of drug [15]. In addition, SPIONs are non-toxic [16] as the iron from degraded NP cores accumulates into the natural iron stores of the body [17]. The high surface area to volume ratio of nanomaterials, such as liposomes and solid core NPs including SPIONs, provides the potential for high drug loading and attachment of other surface constituents such as tumor-targeting ligands. Attachment of the chemotherapeutic methotrexate to SPIONs provided both contrast in MRI and controlled drug delivery to breast cancer, cervical cancer, and glioma cells *in vitro* [18,19]. SPIONs and DOX have been loaded into polymeric micelles for liver cancer theranostics and showed minimal side-effects as compared to free DOX and the Doxil formulation in a rabbit model [20]. DOX physically adsorbed to SPIONs for MR imaging and therapy of a mouse model of Lewis lung carcinoma had excellent antitumor effects (63% reduction in tumor growth) with no systemic toxicity [21]. Another study showed that daunorubicin loaded SPIONs increased the intracellular accumulation of drug in drug resistant leukemia cells, but their therapeutic advantage was unclear [22,23]. These and other [24–28] studies with drug loaded SPIONs demonstrate their advantage as drug delivery vehicles by increasing intracellular drug concentration and minimizing off-target side effects. However, no study to date has determined if drug loaded SPIONs are able to overcome MDR for improved treatment efficacy.

We previously developed SPIONs coated with polyethylene glycol (PEG) that show long-term stability in biological media and excellent magnetic properties [29]. Based on this work, here we develop a DOX-conjugated SPION (NP-DOX) and examine its susceptibility to MDR-mediated drug efflux, a common mechanism of resistance to DOX [30]. DOX is conjugated via a pH sensitive hydrazone bond to control intracellular release and facilitate nuclear uptake [31]. The nanoparticle (NP) utilizes polyethylenimine (PEI) as a docking molecule for DOX to achieve high drug loading and as a strategy to escape endosomal retention in order to increase the intracellular DOX concentration [32]. Low molecular weight PEI is less toxic than high molecular weight PEIs [33], and conjugation to biocompatible polymers (such as PEG on NP) greatly reduces its toxicity [34,35] while maintaining a significant buffering capacity [36–39]. We show that NP-DOX is resistant to ABC-mediated drug efflux, and that increased drug retention is accompanied by enhanced loss of viability.

2. Materials and methods

2.1. Materials

Doxorubicin-HCl, PEI (1.2 kDa), and all other chemicals were purchased from Sigma-Aldrich (St. Louis, MO) unless otherwise specified. The heterobifunctional linkers 2-iminothiolane (Traut's reagent), succinimidyl iodoacetate (SIA), and β-maleimidopropionic acid hydrazide (BMPH) were purchased from Molecular Biosciences (Boulder, CO). Tissue culture reagents including Dulbecco's modified Eagle medium (DMEM) and antibiotic–antimycotic were purchased from Invitrogen (Carlsbad, CA). Fetal bovine serum (FBS) was purchased from Atlanta Biologicals (Lawrenceville, GA).

2.2. Nanoparticle synthesis

Iron oxide NPs coated with a monolayer of amine terminated PEG (SPION) were prepared as previously described and stored at 4 °C in PBS [29]. DOX was covalently attached to PEI as outlined in Fig. 1. PEI (1 mg) was thiolated using Traut's reagent (1 mg) in 100 μL of 100 mM sodium bicarbonate, pH 8.0, 5 mM EDTA. After a one-hour incubation at room temperature, 2.2 mg of BMPH in 100 μL dimethylformamide (DMF) was added to thiolated PEI, followed by 4 mg of DOX in 200 μL DMF. The reaction was maintained in the dark at room temperature for 2 hrs. In a separate reaction, 6 mg of SPIONs in 1.16 mL PBS was incubated with 6 mg SIA in 133 μL DMF in the dark with gentle rocking to produce a thiol reactive iodoacetyl group. Unreacted SIA was removed by size exclusion chromatography using a PD-10 desalting column (GE Healthcare, Piscataway, NJ) equilibrated with 100 mM sodium bicarbonate, pH 8.0, 5 mM EDTA. The PEI-linked DOX and SIA derivatized SPIONs were incubated with gentle rocking in the dark for 2 h, and NPs were separated from unreacted precursors by size exclusion chromatography using S-200 resin (GE Healthcare, Piscataway, NJ) equilibrated with PBS. DOX-conjugated SPIONs (NP-DOX) were stored in PBS at 4 °C in the dark.

2.3. Nanoparticle characterization

The size and zeta potential were determined using a DTS Zetasizer Nano (Malvern Instruments, Worcestershire, UK) by measuring dynamic light scattering of a 100 μg/mL suspension of NP-DOX at pH 7.4. The stability of NP-DOX was determined at 100 μg/mL in DMEM containing 10% FBS and 1% antibiotic–antimycotic. DOX content was determined by measuring fluorescence of NP-DOX dissolved in concentrated HCl using a SpectraMax M5 microplate reader (Molecular Devices, Union City, CA) at excitation and emission wavelengths of 485 nm and 590 nm, respectively. NP-DOX were placed in an equal volume of concentrated HCl to dissolve the iron oxide core. The number of DOX per NP was calculated based on a standard curve of DOX fluorescence to DOX concentration, and assuming a NP core size of 12 nm, as determined previously, to estimate NP molecular weight [29]. The number of PEI molecules per NP was determined using proton NMR on a Bruker AVance spectrometer operating at 300 MHz with TSP as a reference.

2.4. Drug release

NP-DOX were diluted into PBS at pH 7.5 or 6.5 and acetate buffer at pH 5.5 or 4.5 at a concentration equivalent to 5 μg/mL free DOX (*i.e.* 8.6 μM DOX) and incubated at 37 °C for 1, 2, 4, 8, and 24 h. Free DOX was also diluted in the same buffers to 5 μg/mL and incubated under the same conditions to serve as unbound control. After incubation and centrifugation at 20,000×*g* to pellet NPs, free DOX content in the supernatant was determined by fluorescence measurement as described above. Percent DOX released from NP-DOX was calculated using the fluorescence of free DOX as a standard.

2.5. Drug resistant cell line development and characterization

Rat glioma C6 cells were purchased from American Type Culture Collection (ATCC, Manassas, VA) and maintained at 37 °C in 95%/5% humidified air/CO_2 in DMEM containing 10% FBS and 1% antibiotic–antimycotic. DOX resistant C6 cells (C6-ADR) were developed by exposing C6 cells to increasing doses (1, 5, 10, 25, 50, 100, 500, 1000, and 5000 ng/mL) of DOX for 24 h followed by 3–4 days of recovery before exposing to the next dose. C6-ADR were then frozen and stored

Table 1
Comparative expression level of MDR-related genes for C6 and C6-ADR cell populations.

	IC_{50} (ng/mL DOX)[a]	ABCB1[b]	ABCB5[b]	ABCB8[b]	ABCC1[b]
C6	455	1 ± 0.03	1 ± 0.2	1 ± 0.03	1 ± 0.02
C6-ADR	>10,000	97 ± 7	7.3 ± 1.8	2.3 ± 0.11	2.8 ± 0.04

Viability assessed by reduction of Alamar blue following the manufacturer's protocol (Invitrogen, Carlsbad, CA). Primers for the ATP-binding cassette (ABC) transporters involved in DOX efflux [30] were designed using Primer-BLAST (NCBI, Bethesda, MD) and purchased from Integrated DNA Technologies (IDT, San Diego, CA).

[a] IC_{50} for DOX was calculated using a polynomial dose–response approximation using the Origin software package (OriginLab Corporation, Northampton, MA).

[b] Expression of ABC transporters was relative to the housekeeping gene GAPDH and was normalized to that of drug sensitive C6 cells.

Table 2
Physiochemical properties and physical characterizations of NP-DOX.

Z-average size (nm)	Volume-average size (nm)	Number-average size (nm)	Zeta potential (mV)	DOX per NP
91	63	30	-2.86 ± 6.80	1089 ± 21

in liquid nitrogen. Fresh aliquots of C6-ADR were used in all experiments to ensure that C6-ADR did not revert to a drug sensitive phenotype. As illustrated in Table 1, the DOX dose required to reduce viability 50% (IC_{50}) was more than 20-fold greater in C6-ADR compared to its wild-type progenitor. Real time PCR revealed that greater drug resistance was accompanied by 2.3- to 97-fold greater abundance of message for the MDR genes ABCB1, ABCB5, ABCB8 and ABCC1 (Table 1), suggesting that elevated resistance to DOX reflected enhanced drug efflux.

2.6. Cellular uptake of NP-DOX

Cells were plated at 100,000 cells in 1 mL supplemented DMEM per well in 24-well plates the night before treatment. Cells were incubated with 1000 ng/mL free DOX or a concentration of NP-DOX equivalent to 1000 ng/mL free drug in 1 mL supplemented medium for 4 h before washing the cells thrice with PBS and returning them to the drug-free medium. Cell number per well was determined using Alamar blue and calculated based on a previously prepared standard curve of Alamar blue reduction to plated cell number. At 4 h and 24 h time points after initiating drug treatment, cells were solubilized with 400 μL concentrated HCl then transferred to a black bottom 96-well plate for fluorescence measurement on the microplate reader. DOX concentration per cell was calculated based on DOX fluorescence and cell number obtained from Alamar blue reduction.

2.7. Fluorescence imaging

Cells were plated at 500,000 cells in 2 mL supplemented medium per well in 6-well plates containing 22×22 mm glass cover slips the night before treatment. Cells were incubated with 1000 ng/mL free DOX or equimolar concentration of NP-DOX in 2 mL fully supplemented DMEM for 4 h. Cells were subsequently washed thrice with PBS before adding 2 mL of supplemented media. After 24 h, cells were washed thrice with PBS and fixed in 4% formaldehyde (Polysciences Inc., Warrington, PA) for 30 min. Cell membranes were stained with wheat germ agglutinin, Alexa Fluor 488 conjugates (WGA-AF488, Invitrogen, Carlsbad, CA) following the manufacturer's protocol. Cover slips were then mounted on microscope slides using Prolong Gold anti-fade solution (Invitrogen, Carlsbad, CA) containing DAPI for cell nuclei staining. Images were acquired on an inverted fluorescent microscope (Nikon Instruments, Melville, NY) with the appropriate filters using a Nikon Ri1 Color Cooled Camera System (Nikon Instruments, Melville, NY) and 60× Oil Objective Lens (Nikon Instruments, Melville, NY).

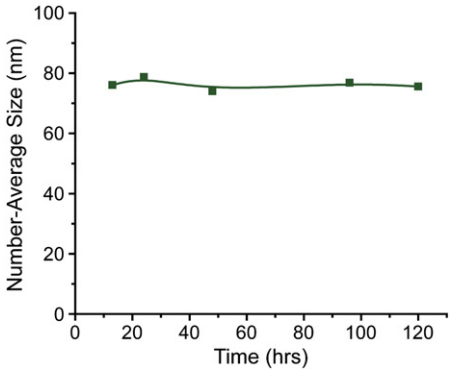

Fig. 2. Colloidal stability of NP-DOX. NP-DOX displayed no appreciable change in size during incubation at 37 °C for 5 days in DMEM with 10% FBS.

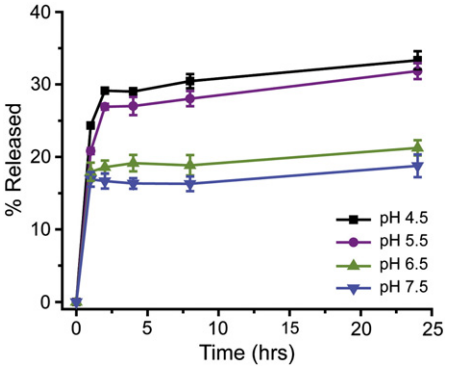

Fig. 3. Drug release profiles showing the pH dependent release of DOX from NP-DOX. The pH tested correspond to that of blood (pH 7.5), tumor microenvironment (pH 6.5), and endosomes/lysosomes (pH 5.5 and 4.5).

2.8. Dose–response experiments

Sensitive C6 and resistant C6-ADR cells were plated at 10,000 cells per well in 96-well plates the night before treatment. Cells were then treated with free DOX or NP-DOX at 0, 10, 50, 100, 1000, and 10,000 ng/mL DOX in 150 μL supplemented DMEM for 4 h before washing thrice with PBS and adding 150 μL fresh medium. Cell viability was determined at 24, 48, and 72 h using the Alamar blue viability assay following the manufacturer's protocol (Invitrogen, Carlsbad, CA). IC_{50} values were calculated from dose–response curves generated using a polynomial dose–response approximation using the Origin software package (OriginLab Corporation, Northampton, MA). The resistance factor was calculated from IC_{50} values at the 72 h time point by dividing the IC_{50} of C6-ADR cells by the IC_{50} of C6 cells. The fold increase in viability (*i.e.* C6-ADR viability/C6 viability) was calculated at the 24, 48, and 72 h after exposure to 1000 ng/mL DOX or NP-DOX.

2.9. Statistical analysis

All experiments were run in triplicate and acquired data are expressed at mean ± SD. Statistical significance was determined using Student's *t*-test. Significant values were designated as follows: $^{*}P<0.05$, $^{**}P<0.01$, and $^{***}P<0.001$.

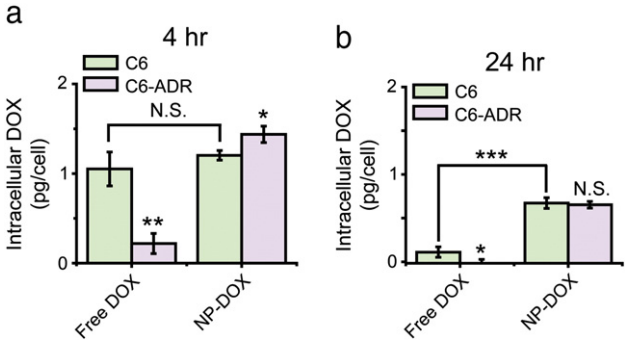

Fig. 4. Accumulation of free DOX or NP-DOX in wild-type and drug-resistant C6 cells. Cells were treated for 4 h with 1000 ng/mL DOX or equimolar concentration of DOX on NP-DOX, then intracellular DOX was determined by the fluorescence of cell lysate and normalized to cell number using Alamar Blue at a) 4 h and b) 24 h after initial drug exposure. N.S. indicates no significance, * indicates $P<0.05$, ** indicates $P<0.01$, and *** indicates $P<0.001$ as determined by Student's *t*-test.

3. Results and discussion

3.1. Nanoparticle development

Iron oxide NPs coated with amine terminated polyethylene glycol (PEG) [29] were derivatized with doxorubicin (DOX) covalently bound to PEI via a pH labile hydrazone bond using a BMPH heterobifunctional linker (NP-DOX; Fig. 1). Using PEI as a linking molecule enabled very high loading of DOX, *i.e.* 1089 ± 21 DOX molecules per NP, quantified by fluorescence. This high loading capacity is critical to minimize the amount of NPs required to deliver cytotoxic drug doses. Furthermore, the use of PEI as the docking molecule provided a mechanism to escape the endosome/lysosome, a likely site of internalization of NPs [5], by preventing exocytosis through the proton sponge effect [40]. These properties are designed to increase therapeutic efficacy in multidrug resistant (MDR) cells by facilitating intracellular delivery of high drug doses.

The size and surface charge of NPs are important physiochemical parameters in designing drug delivery vehicles. NP-DOX had a hydrodynamic size within the desired range of 10–100 nm to prevent elimination by the kidneys (<10 nm) and recognition by macrophage cells (>100 nm) [41,42]. As listed in Table 2, Z-average size, volume average size, and number average size were 91 nm, 63 nm, and 30 nm, respectively. NP-DOX had a slightly negative zeta potential, a measure of the surface charge, (−2.86 ± 6.80) owing to the negative charge of both NP and DOX. This negative zeta potential may facilitate deep penetration of NPs into tumors *in vivo* [43]. However, NPs with volume-average sizes ≥60 nm are not expected to non-specifically penetrate deeply into tumors [44]. Therefore, NP-DOX will require a targeting ligand to achieve significant distribution throughout a tumor *in vivo* [45–47]. These NP properties will facilitate clinical application and are summarized in Table 2.

3.2. Nanoparticle stability

Another important parameter of nano-sized delivery vehicles is their colloidal stability in complex fluids such as blood to prevent aggregation and the potential for embolism. Furthermore, aggregation

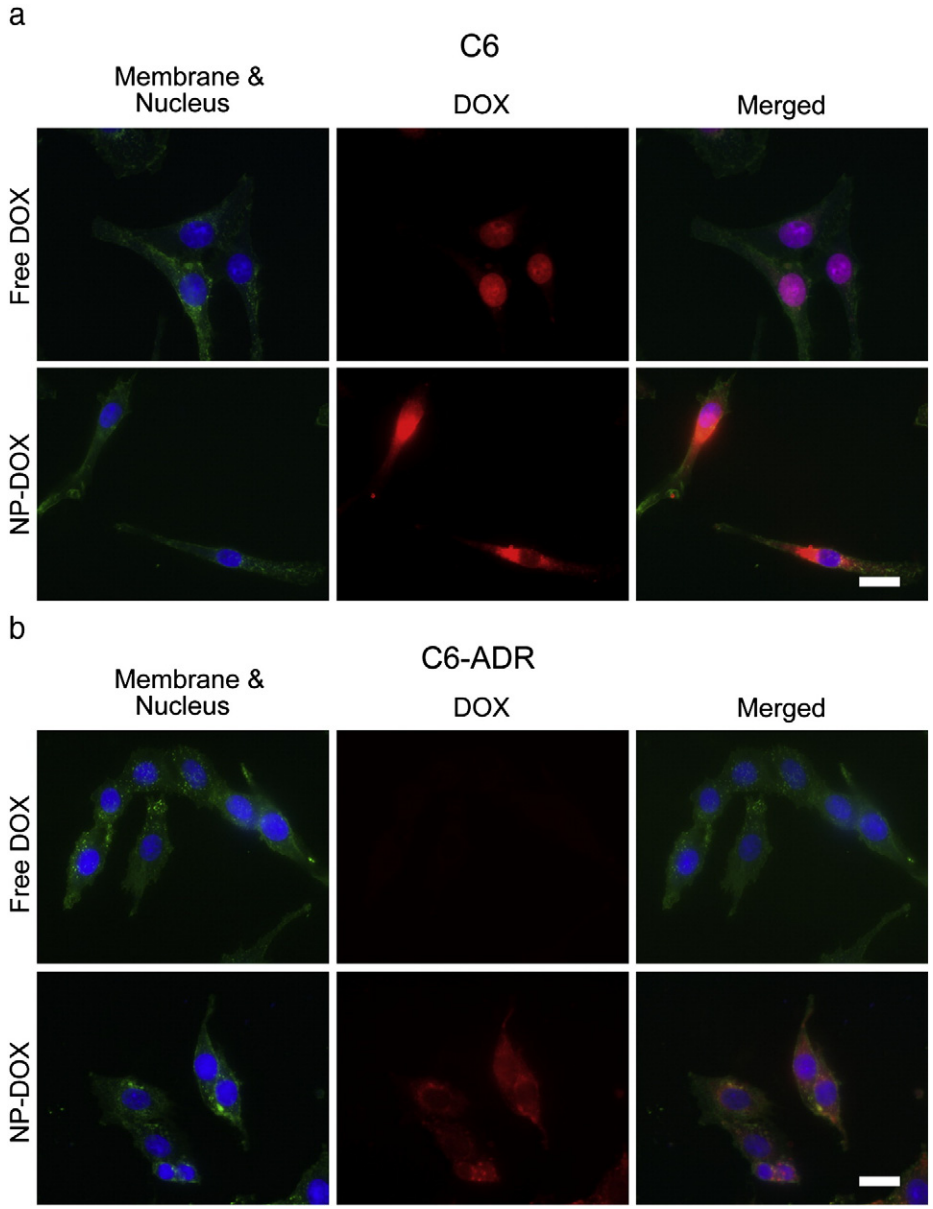

Fig. 5. Fluorescence visualization of DOX intracellular accumulation. Both a) drug sensitive C6 and b) drug resistant C6-ADR cells were treated with 1000 ng/mL free DOX or equivalent DOX concentration of NP-DOX for 4 h then allowed to grow for an additional 20 h. Scale bars correspond to 20 μm.

of NPs could compromise therapeutic efficacy by promoting removal from the circulation by the reticuloendothelial system. NP-DOX showed excellent stability in serum-supplemented DMEM over 5 days (Fig. 2) indicating that the NPs are not prone to aggregation under physiological conditions. The larger number-average size in DMEM containing 10% FBS as compared to PBS (Table 2) indicates that although the colloidal stability of NP-DOX is not affected, the hydrodynamic properties are slightly different, possibly due to the presence of amino acids and globular proteins such as serum albumin.

3.3. pH dependent drug release

NP-DOX was incubated in PBS and acetate buffers at different pH to examine drug release under conditions likely encountered following NP tumor uptake and intracellular sequestration. The pH levels chosen replicated that found in the blood (pH 7.4), as well as the acidity characteristic of the tumor microenvironment (pH 5.8–7.6) [48], and of endosomes/lysosomes which are more acidic (pH 4–6) [49]. As shown in Fig. 3, DOX was released more readily at pH less than 6.5. This 50% improvement in DOX release at acidic pH indicates that DOX can be released preferentially in the endosomal/lysosomal compartment of the cell where it is protected from drug efflux. Fig. 3 also shows that at pH 4.5 only 33% of bound drug is released in 24 h suggesting that hydrophobic interactions may bind a fraction of the DOX to the iron oxide NP core after cleavage of the hydrazone bond [50]. This could account for limited release of DOX from NP-DOX.

3.4. Intracellular accumulation of doxorubicin

To determine if DOX conjugated to NPs could circumvent ABC-mediated drug efflux, we compared DOX accumulation in wild-type C6 glioma cells and in C6-ADR, a DOX-resistant variant that over-expresses a number ABC transporter genes (Table 1). Cells were incubated with 1000 ng/mL free DOX or an equivalent dose of NP-DOX for 4 h before being returned to the drug-free, fresh medium. As shown in Fig. 4a, after drug treatment (*i.e.*, 4 h after initial drug exposure), accumulation of free DOX in wild-type cells was 5-fold greater compared to drug resistant cells (C6-ADR) (1.05 ± 0.19 pg *vs* 0.22 ± 0.11 pg DOX/cell; $P \leq 0.01$). By 24 h after initial drug exposure, DOX concentration in C6 cells treated with free drug (0.11 ± 0.06 pg DOX/cell) was about 10-fold lower than at 4 h (1.05 ± 0.19 pg DOX/cell) likely reflecting drug metabolism and efflux [51], while DOX was undetectable (-0.02 ± 0.04 pg DOX/cell) in C6-ADR cells (Fig. 4b). These findings indicate that ABC transporter gene over-expression impedes DOX accumulation in C6 cells.

In contrast to free drug, accumulation of DOX conjugated to NPs did not differ between C6 and C6-ADR cells either 4 h (1.20 ± 0.05 pg *vs* 1.44 ± 0.09 pg DOX/cell; Fig. 4a) or 24 h (0.67 ± 0.06 pg *vs* 0.65 ± 0.04 pg DOX/cell; Fig. 4b) after initial drug exposure. These results indicate that NP-DOX is less susceptible to ABC-mediated drug efflux. The greater accumulation achieved by NP-DOX may also reflect diminished drug metabolism. DOX is reduced by aldo-keto reductases (AKR), a class of enzymes that facilitate the conversion of hydrophobic substrates into alcohols (e.g., doxorubicinol) as an initial step in detoxification [52]. NP-DOX is not a substrate for AKRs since the relevant ketone groups of DOX are linked to PEI via hydrazone bonds (Fig. 1). Importantly, AKR-mediated reduction has been implicated in the life-threatening cardiotoxicity associated with DOX [52,53], suggesting that conjugation of DOX to NPs could reduce the risk of cardiotoxicity.

To further characterize drug uptake and accumulation in cells, the intracellular localization of DOX in C6 and C6-ADR cells treated for 4 h with either free DOX or NP-DOX was visualized by fluorescence imaging 20 h after drug exposure (Fig. 5). Free DOX accumulated in the nucleus of C6 cells while NP-DOX accumulated throughout the cell and concentrated in the perinuclear region (Fig. 5a). In contrast, no fluorescence was detectable in resistant C6-ADR cells treated with free DOX, consistent with enhanced drug efflux mediated by the overexpression of ABC transporters, in accord with previous studies using cells displaying the MDR phenotype [31,54] (Fig. 5b). In contrast, NP-DOX was detectable in C6-ADR cells further suggesting that DOX conjugated NPs is not a substrate for drug efflux (Fig. 5b).

3.5. Overcoming MDR for increased therapeutic efficacy

To examine the susceptibility of NP-DOX to MDR, the viability of C6-ADR cells was determined using the Alamar Blue assay at 24, 48, and 72 h after initiating exposure to either free DOX or NP-DOX (Fig. 6b). C6-ADR cells were more sensitive to NP-DOX than to free drug, suggesting that NP-DOX can circumvent drug-efflux-mediated drug resistance. Drug sensitive C6 cells were more sensitive to free DOX (Fig. 6a) which is likely due to free DOX quickly diffusing to the

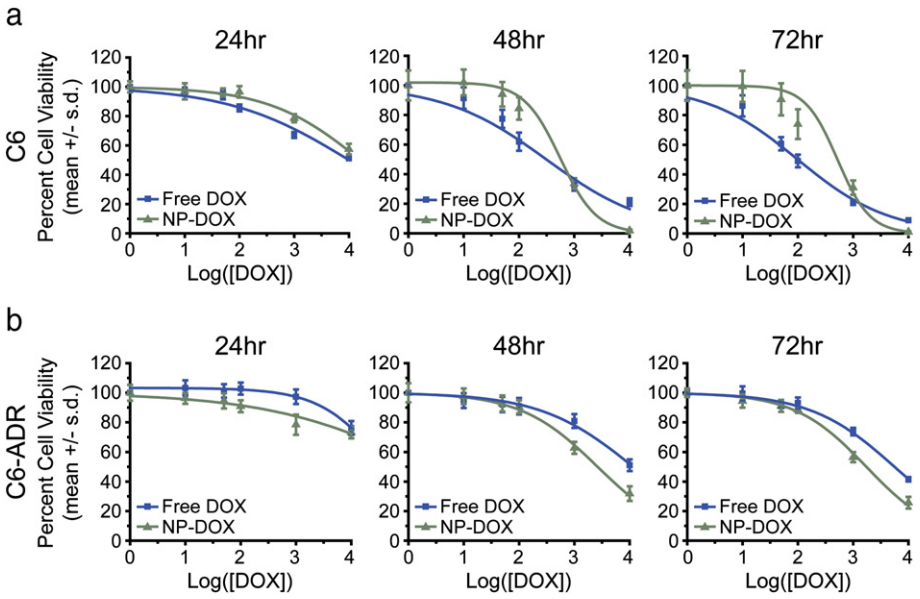

Fig. 6. Drug response curves. a) C6 and b) C6-ADR were treated with free DOX or NP-DOX and cell viability was analyzed 24, 48, and 72 h post-treatment. DOX concentrations are in ng/mL.

Table 3
IC_{50} values for free DOX and NP-DOX in sensitive C6 and resistant C6-ADR glioma cells at 24, 48, and 72 h time points. IC_{50} values are given in ng/mL doxorubicin.

		Free DOX	NP-DOX	P-value
C6	24 h	>10,000	>10,000	n.a.
	48 h	311 ± 18	554 ± 9	<0.001
	72 h	99 ± 4	521 ± 17	<0.001
C6-ADR	24 h	>10,000	>10,000	n.a.
	48 h	>10,000	2623 ± 28	<0.001
	72 h	5568 ± 40	1728 ± 25	<0.001

nucleus, whereas NP-DOX must be trafficked through the cell before free DOX is released and can reach the nucleus to intercalate DNA. These trends in drug response are more clearly illustrated by the IC_{50} values obtained from the dose–response curves that were approximately 3- to 5-times lower for NP-DOX than for free DOX in C6-ADR cells (Table 3). This provides evidence that the ability of NP-DOX to prevent drug efflux from drug-resistant cells corresponds to enhanced cell kill. Furthermore, the IC50 values are well within the range achievable in blood plasma, suggesting their clinical applicability. Clinically, the PEGylated liposome nanoparticle formulation of DOX, Doxil, achieves peak plasma concentrations of 9–45 μg/mL for well over 4 h (the amount of time cells were exposed to drug in our study) [55].

Comparing the viability of C6-ADR to C6 cells treated with 1000 ng/mL of DOX or NP-DOX further indicates that NP conjugated drug is less susceptible to MDR than free drug. As shown in Fig. 7a, the increase in drug resistance conferred by overexpression of ABC transporter genes is consistently less for NP-DOX treatment than for free DOX treatment. Further evidence of NP-DOX circumventing drug efflux-mediated resistance is provided by comparing the ratio of IC_{50} values for C6-ADR and C6 cells treated with free DOX and NP-DOX. As shown in Fig. 7b, this ratio, or resistance factor, for free drug was 56 ± 2.3 (*i.e.*, the IC_{50} for C6-ADR was 56-fold greater than that for C6). In contrast, the ratio for NP-DOX was approximately 10-fold lower (3.3 ± 0.1), consistent with NP-DOX being less susceptible to drug efflux than free drug.

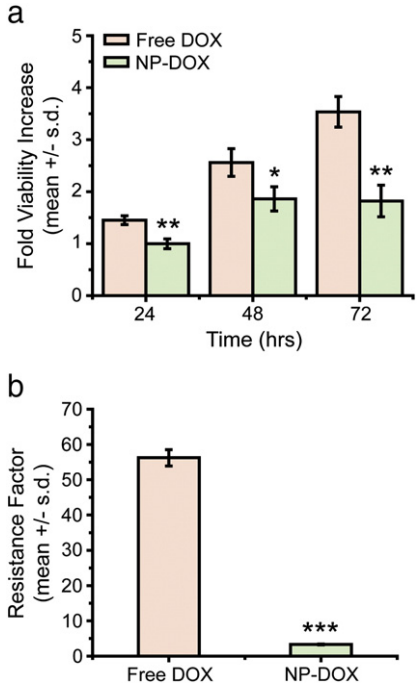

Fig. 7. NP-DOX circumvents MDR-mediated resistance. a) Fold increase in viability of drug-resistant cells relative to drug-sensitive cells (C6-ADR/C6) treated with 1000 ng/mL free DOX or equivalent dose of NP-DOX. b) Resistance factors for 72 h time point. The resistance factor is the ratio of IC_{50} of C6-ADR to the IC_{50} of C6. N.S. indicates no significance, * indicates $P<0.05$, ** indicates $P<0.01$, and *** indicates $P<0.001$ as determined by Student's *t*-test.

4. Conclusions

Superparamagnetic iron oxide NPs loaded with covalently bound, biologically active DOX using the pH labile hydrazone bond were successfully prepared. Very high loading of DOX was achieved through the use of polyethylenimine as a docking molecule. DOX loaded NPs showed greatest release at pH between 4 and 5, comparable to that found in endosomes/lysosomes. Importantly, NP-DOX was able to circumvent the drug resistance associated with overexpression of ATP-binding cassette (ABC) transporters, specifically ABCB1, ABCB5, ABCB8, and ABCC1, in C6 glioma cells, suggesting a role for NP-conjugated drugs in overcoming ABC-mediated drug resistance. This nanoparticle system could provide an effective therapy for patients afflicted with deadly drug-resistant cancers who would otherwise not respond favorably.

Acknowledgements

This work was supported in part by NIH grants NIH/NCI R01CA119408 and R01EB006043. We acknowledge the support of the NIH training grant (T32CA138312) for FK and NCI/NSF IGERT fellowship for CF. We also thank Joseph Ayesh, Surya Kotha, and Andrea Nordberg for laboratory assistance.

References

[1] M.M. Gottesman, T. Fojo, S.E. Bates, Multidrug resistance in cancer: role of ATP-dependent transporters, Nat. Rev. Cancer 2 (1) (2002) 48–58.
[2] G. Szakacs, J.K. Paterson, J.A. Ludwig, C. Booth-Genthe, M.M. Gottesman, Targeting multidrug resistance in cancer, Nat. Rev. Drug Discov. 5 (3) (2006) 219–234.
[3] C. Sun, J.S. Lee, M. Zhang, Magnetic nanoparticles in MR imaging and drug delivery, Adv. Drug Deliv. Rev. 60 (11) (2008) 1252–1265.
[4] M.E. Davis, Z. Chen, D.M. Shin, Nanoparticle therapeutics: an emerging treatment modality for cancer, Nat. Rev. Drug Discov. 7 (9) (2008) 771–782.
[5] O. Veiseh, J.W. Gunn, M. Zhang, Design and fabrication of magnetic nanoparticles for targeted drug delivery and imaging, Adv. Drug Deliv. Rev. 62 (3) (2010) 284–304.
[6] S. Nobili, I. Landini, B. Giglioni, E. Mini, Pharmacological strategies for overcoming multidrug resistance, Curr. Drug Targets 7 (7) (2006) 861–879.
[7] Y. Malam, M. Loizidou, A.M. Seifalian, Liposomes and nanoparticles: nanosized vehicles for drug delivery in cancer, Trends Pharmacol. Sci. 30 (11) (2009) 592–599.
[8] Y.P. Hu, N. Henry-Toulme, J. Robert, Failure of liposomal encapsulation of doxorubicin to circumvent multidrug resistance in an *in vitro* model of rat glioblastoma cells, Eur. J. Cancer 31A (3) (1995) 389–394.
[9] E. Garcion, A. Lamprecht, B. Heurtault, A. Paillard, A. Aubert-Pouessel, B. Denizot, P. Menei, J.P. Benoit, A new generation of anticancer, drug-loaded, colloidal vectors reverses multidrug resistance in glioma and reduces tumor progression in rats, Mol. Cancer Ther. 5 (7) (2006) 1710–1722.
[10] L.S. Jabr-Milane, L.E. van Vlerken, S. Yadav, M.M. Amiji, Multi-functional nanocarriers to overcome tumor drug resistance, Cancer Treat. Rev. 34 (7) (2008) 592–602.
[11] X. Dong, R.J. Mumper, Nanomedicinal strategies to treat multidrug-resistant tumors: current progress, Nanomedicine (Lond) 5 (4) (2010) 597–615.
[12] V.I. Shubayev, T.R. Pisanic, S.H. Jin, Magnetic nanoparticles for theragnostics, Adv. Drug Deliv. Rev. 61 (6) (2009) 467–477.
[13] M. Arruebo, R. Fernández-Pacheco, M.R. Ibarra, J. Santamaría, Magnetic nanoparticles for drug delivery, Nano Today 2 (3) (2007) 22–32.
[14] C. Fang, M. Zhang, Nanoparticle-based theragnostics: integrating diagnostic and therapeutic potentials in nanomedicine, J. Control. Release 146 (1) (2010) 2–5.
[15] T. Lammers, F. Kiessling, W.E. Hennink, G. Storm, Nanotheranostics and image-guided drug delivery: current concepts and future directions, Mol. Pharm. 7 (6) (2010) 1899–1912.
[16] C. Sun, K. Du, C. Fang, N. Bhattarai, O. Veiseh, F. Kievit, Z. Stephen, D. Lee, R.G. Ellenbogen, B. Ratner, M. Zhang, PEG-mediated synthesis of highly dispersive multifunctional superparamagnetic nanoparticles: their physicochemical properties and function in vivo, ACS Nano 4 (4) (2010) 2402–2410.
[17] R. Weissleder, D.D. Stark, B.L. Engelstad, B.R. Bacon, C.C. Compton, D.L. White, P. Jacobs, J. Lewis, Superparamagnetic iron oxide: pharmacokinetics and toxicity, AJR Am. J. Roentgenol. 152 (1) (1989) 167–173.
[18] N. Kohler, C. Sun, A. Fichtenholtz, J. Gunn, C. Fang, M. Zhang, Methotrexate-immobilized poly(ethylene glycol) magnetic nanoparticles for MR imaging and drug delivery, Small 2 (6) (2006) 785–792.

[19] N. Kohler, C. Sun, J. Wang, M. Zhang, Methotrexate-modified superparamagnetic nanoparticles and their intracellular uptake into human cancer cells, Langmuir 21 (19) (2005) 8858–8864.

[20] J.H. Maeng, D.H. Lee, K.H. Jung, Y.H. Bae, I.S. Park, S. Jeong, Y.S. Jeon, C.K. Shim, W. Kim, J. Kim, J. Lee, Y.M. Lee, J.H. Kim, W.H. Kim, S.S. Hong, Multifunctional doxorubicin loaded superparamagnetic iron oxide nanoparticles for chemotherapy and magnetic resonance imaging in liver cancer, Biomaterials 31 (18) (2010) 4995–5006.

[21] M.K. Yu, Y.Y. Jeong, J. Park, S. Park, J.W. Kim, J.J. Min, K. Kim, S. Jon, Drug-loaded superparamagnetic iron oxide nanoparticles for combined cancer imaging and therapy in vivo, Angew. Chem. Int. Ed Engl. 47 (29) (2008) 5362–5365.

[22] X. Wang, R. Zhang, C. Wu, Y. Dai, M. Song, S. Gutmann, F. Gao, G. Lv, J. Li, X. Li, Z. Guan, D. Fu, B. Chen, The application of Fe_3O_4 nanoparticles in cancer research: a new strategy to inhibit drug resistance, J. Biomed. Mater. Res. A 80 (4) (2007) 852–860.

[23] B.A. Chen, J. Cheng, Y.A. Wu, F. Gao, W.L. Xu, H.L. Shen, J.H. Ding, C. Gao, Q. Sun, X.C. Sun, H.Y. Cheng, G.H. Li, W.J. Chen, N.N. Chen, L.J. Liu, X.M. Li, X.M. Wang, Reversal of multidrug resistance by magnetic Fe_3O_4 nanoparticle copolymerizating daunorubicin and 5-bromotetrandrine in xenograft nude-mice, Int. J. Nanomed. 4 (1) (2009) 73–78.

[24] T.K. Jain, M.A. Morales, S.K. Sahoo, D.L. Leslie-Pelecky, V. Labhasetwar, Iron oxide nanoparticles for sustained delivery of anticancer agents, Mol. Pharm. 2 (3) (2005) 194–205.

[25] C. Alexiou, R.J. Schmid, R. Jurgons, M. Kremer, G. Wanner, C. Bergemann, E. Huenges, T. Nawroth, W. Arnold, F.G. Parak, Targeting cancer cells: magnetic nanoparticles as drug carriers, Eur. Biophys. J. 35 (5) (2006) 446–450.

[26] A.M. Derfus, G. von Maltzahn, T.J. Harris, T. Duza, K.S. Vecchio, E. Ruoslahti, S.N. Bhatia, Remotely triggered release from magnetic nanoparticles, Adv. Mater. 19 (22) (2007) 3932–3936.

[27] J. Yang, C.H. Lee, H.J. Ko, J.S. Suh, H.G. Yoon, K. Lee, Y.M. Huh, S. Haam, Multifunctional magneto-polymeric nanohybrids for targeted detection and synergistic therapeutic effects on breast cancer, Angew. Chem. Int. Ed Engl. 46 (46) (2007) 8836–8839.

[28] J.R. Lai, Y.W. Chang, H.C. Yen, N.Y. Yuan, M.Y. Liao, C.Y. Hsu, J.L. Tsai, P.S. Lai, Multifunctional doxorubicin/superparamagnetic iron oxide-encapsulated Pluronic F127 micelles used for chemotherapy/magnetic resonance imaging, J. Appl. Phys. 107 (9) (2010) 3.

[29] C. Fang, N. Bhattarai, C. Sun, M. Zhang, Functionalized nanoparticles with long-term stability in biological media, Small 5 (14) (2009) 1637–1641.

[30] J.I. Fletcher, M. Haber, M.J. Henderson, M.D. Norris, ABC transporters in cancer: more than just drug efflux pumps, Nat. Rev. Cancer 10 (2) (2010) 147–156.

[31] X.B. Xiong, Z. Ma, R. Lai, A. Lavasanifar, The therapeutic response to multifunctional polymeric nano-conjugates in the targeted cellular and subcellular delivery of doxorubicin, Biomaterials 31 (4) (2010) 757–768.

[32] E.S. Lee, K. Na, Y.H. Bae, Doxorubicin loaded pH-sensitive polymeric micelles for reversal of resistant MCF-7 tumor, J. Control. Release 103 (2) (2005) 405–418.

[33] D. Fischer, T. Bieber, Y. Li, H.P. Elsasser, T. Kissel, A novel non-viral vector for DNA delivery based on low molecular weight, branched polyethylenimine: effect of molecular weight on transfection efficiency and cytotoxicity, Pharm. Res. 16 (8) (1999) 1273–1279.

[34] F.M. Kievit, O. Veiseh, N. Bhattarai, C. Fang, J.W. Gunn, D. Lee, R.G. Ellenbogen, J.M. Olson, M. Zhang, PEI-PEG-chitosan copolymer coated iron oxide nanoparticles for safe gene delivery: synthesis, complexation, and transfection, Adv. Funct. Mater. 19 (14) (2009) 2244–2251.

[35] O. Veiseh, F.M. Kievit, J.W. Gunn, B.D. Ratner, M. Zhang, A ligand-mediated nanovector for targeted gene delivery and transfection in cancer cells, Biomaterials 30 (4) (2009) 649–657.

[36] H. Kim, H.A. Kim, Y.M. Bae, J.S. Choi, M. Lee, Dexamethasone-conjugated polyethylenimine as an efficient gene carrier with an anti-apoptotic effect to cardiomyocytes, J. Gene Med. 11 (6) (2009) 515–522.

[37] M.R. Rekha, C.P. Sharma, Hemocompatible pullulan-polyethyleneimine conjugates for liver cell gene delivery: *in vitro* evaluation of cellular uptake, intracellular trafficking and transfection efficiency, Acta Biomater. 7 (1) (2011) 370–379.

[38] K. Ma, M. Hu, M. Xie, H. Shen, L. Qiu, W. Fan, H. Sun, S. Chen, Y. Jin, Investigation of polyethylenimine-grafted-triamcinolone acetonide as nucleus-targeting gene delivery systems, J. Gene Med. 12 (8) (2010) 669–680.

[39] L.Y. Su, T.Y. Fang, W.C. Tseng, The effect of pendant hydrophobicity on the biological efficacy of polyethylenimine conjugate, Biochem. Eng. J. 49 (1) (2010) 21–27.

[40] O. Boussif, F. Lezoualc'h, M.A. Zanta, M.D. Mergny, D. Scherman, B. Demeneix, J.P. Behr, A versatile vector for gene and oligonucleotide transfer into cells in culture and in vivo: polyethylenimine, Proc. Natl Acad. Sci. USA 92 (16) (1995) 7297–7301.

[41] F. Alexis, E. Pridgen, L.K. Molnar, O.C. Farokhzad, Factors affecting the clearance and biodistribution of polymeric nanoparticles, Mol. Pharm. 5 (4) (2008) 505–515.

[42] M. Longmire, P.L. Choyke, H. Kobayashi, Clearance properties of nano-sized particles and molecules as imaging agents: considerations and caveats, Nanomedicine 3 (5) (2008) 703–717.

[43] B. Kim, G. Han, B.J. Toley, C.K. Kim, V.M. Rotello, N.S. Forbes, Tuning payload delivery in tumour cylindroids using gold nanoparticles, Nat. Nanotechnol. 5 (6) (2010) 465–472.

[44] Z. Popovic, W. Liu, V.P. Chauhan, J. Lee, C. Wong, A.B. Greytak, N. Insin, D.G. Nocera, D. Fukumura, R.K. Jain, M.G. Bawendi, A nanoparticle size series for in vivo fluorescence imaging, Angew. Chem. Int. Ed Engl. 49 (46) (2010) 8649–8652.

[45] F.M. Kievit, O. Veiseh, C. Fang, N. Bhattarai, D. Lee, R.G. Ellenbogen, M. Zhang, Chlorotoxin labeled magnetic nanovectors for targeted gene delivery to glioma, ACS Nano 4 (8) (2010) 4587–4594.

[46] D.W. Bartlett, H. Su, I.J. Hildebrandt, W.A. Weber, M.E. Davis, Impact of tumor-specific targeting on the biodistribution and efficacy of siRNA nanoparticles measured by multimodality *in vivo* imaging, Proc. Natl Acad. Sci. USA 104 (39) (2007) 15549–15554.

[47] C.H. Choi, C.A. Alabi, P. Webster, M.E. Davis, Mechanism of active targeting in solid tumors with transferrin-containing gold nanoparticles, Proc. Natl Acad. Sci. USA 107 (3) (2010) 1235–1240.

[48] T. Mashima, S. Sato, Y. Sugimoto, T. Tsuruo, H. Seimiya, Promotion of glioma cell survival by acyl-CoA synthetase 5 under extracellular acidosis conditions, Oncogene 28 (1) (2009) 9–19.

[49] M. Guo, Y. Yan, X.Z. Liu, H.S. Yan, K.L. Liu, H.K. Zhang, Y.J. Cao, Multilayer nanoparticles with a magnetite core and a polycation inner shell as pH-responsive carriers for drug delivery, Nanoscale 2 (3) (2010) 434–441.

[50] S.K. Agrawal, N. Sanabria-DeLong, J.M. Coburn, G.N. Tew, S.R. Bhatia, Novel drug release profiles from micellar solutions of PLA–PEO–PLA triblock copolymers, J. Control. Release 112 (1) (2006) 64–71.

[51] X. Decleves, S. Bihorel, M. Debray, S. Yousif, G. Camenisch, J.M. Scherrmann, ABC transporters and the accumulation of imatinib and its active metabolite CGP74588 in rat C6 glioma cells, Pharmacol. Res. 57 (3) (2008) 214–222.

[52] Y. Jin, T.M. Penning, Aldo-keto reductases and bioactivation/detoxication, Annu. Rev. Pharmacol. Toxicol. 47 (2007) 263–292.

[53] P. Menna, E. Salvatorelli, G. Minotti, Cardiotoxicity of antitumor drugs, Chem. Res. Toxicol. 21 (5) (2008) 978–989.

[54] F. Shen, S. Chu, A.K. Bence, B. Bailey, X. Xue, P.A. Erickson, M.H. Montrose, W.T. Beck, L.C. Erickson, Quantitation of doxorubicin uptake, efflux, and modulation of multidrug resistance (MDR) in MDR human cancer cells, J. Pharmacol. Exp. Ther. 324 (1) (2008) 95–102.

[55] O. Lyass, B. Uziely, R. Ben-Yosef, D. Tzemach, N.I. Heshing, M. Lotem, G. Brufman, A. Gabizon, Correlation of toxicity with pharmacokinetics of pegylated liposomal doxorubicin (Doxil) in metastatic breast carcinoma, Cancer 89 (5) (2000) 1037–1047.